

ScienceDirect

Procedia CIRP 125 (2024) 66-71



CIRP BioM 2024

Finite Element Analysis for the Virtual Surgical Planning of Stiffnessmatched Personalized Load-bearing Percutaneous Implants

Luis H. Olivas-Alanis^a, Michela Sanguedolce^{a,b}, Jason M. Souza^c, David Dean^{a,c,*}

- Department of Materials Science and Engineering, The Ohio State University, 140 W 19th Ave, Columbus, OH. 43210 USA
- Department of Mechanical, Energy and Management Engineering, via Pietro Bucci University of Calabria, Rende, CS, 87036 Italy c

Department of Reconstructive and Plastic Surgery, The Ohio State University, 915 Olentangy River Rd., Columbus, OH 43212 USA *Corresponding author. E-mail address: dean.1016@osu.edu

Abstract

Osseointegrated, percutaneous intramedullary abutments provide a new opportunity to increase freedom of movement, dexterity, and power of prosthetic upper and lower extremities. Device deployment is based on the physician's experience and judgment as no biomechanical information is available or choice of implant location, shape, and materials. Furthermore, there is little opportunity for personalization to improve performance and reduce the risk of stress shielding-induced bone loss or stress concentration-induced device failure. We present a Virtual Surgical Planning (VSP) environment for assessing the expected mechanical outcome of physician choice in the placement site of a percutaneous implant. Starting from de-identified patient images, a virtual anatomical model is created to emulate the surgical implantation procedure. After digitally implanting the intramedullary component-abutment system, the mechanical performance is computationally evaluated via Finite Element Analysis (FEA) under representative in vivo static loading conditions. Our computational analysis includes two different materials for the implant: medical-grade Surgical Grade 5 Titanium alloy (Ti-6Al-4V) and super-elastic Nickel-Titanium (NiTi). The resulting analysis can inspire future design personalization and deployment in an open surgical procedure. Our VSP approach would allow interactive assessment of device location, materials, and performance to alter the normal stress-strain distribution in the bone, potentially avoiding stress shielding and device failure. Future stiffness-matching strategies (e.g., incorporation of internal porosity, new materials, or novel implant geometry), and their effect on implant strength could be evaluated in our computational model.

© 2024 The Authors. Published by Elsevier B.V.
This is an open access article under the CC BY-NC-ND license (https://creativecommons.org/licenses/by-nc-nd/4.0)
Peer-review under responsibility of the scientific committee of the CIRP BioM 2024

Keywords: Percutaneous Implant; Virtual Surgical Planning; Stiffness Matching; Finite Element Modeling; Nickel-Titanium

Nomenclature

TFA Trans-Femoral Amputation

OPRA Osseointegrated Prostheses for the Rehabilitation of

Amputees

Ti64 Titanium-6Aluminum-4Vanadium, Ti-6Al-4V

VSP Virtual Surgical Planning

STL Stereolithography

NiTi Nickel-Titanium alloy

FEA Finite Element Analysis

DOF Degrees of Freedom

1. Introduction

The most common treatment to restore a patient's mobility after Trans-Femoral Amputation (TFA) is the use of a prosthetic limb attached to a plastic socket, fitted to the residual stump. However, in most cases, pain, reduced motion, sensory feedback loss, and soft tissue problems are reported due to pressure on the skin and soft tissues separating the remaining bone and the prosthetic, inconsistent socket fit, and load transferred through the skin-to-prosthesis interface [1], [2].

2212-8271 © 2024 The Authors. Published by Elsevier B.V.

This is an open access article under the CC BY-NC-ND license (https://creativecommons.org/licenses/by-nc-nd/4.0) Peer-review under responsibility of the scientific committee of the CIRP BioM 2024 10.1016/j.procir.2024.08.012

In the last two decades, direct osseous attachment of percutaneous, intramedullary abutments, commonly used in dental and maxillofacial prostheses, has been applied for larger and more complex load-bearing prosthetic limbs [3]. In TFA, one of the most common commercially available percutaneous devices is the Osseointegrated Prostheses for the Rehabilitation of Amputees (OPRATM) Implant System, shown in Figure 1. Thanks to the reduced implant length, this skeletal fixation system is suitable for patients with a relatively short residual stump [4]. The OPRATM device consists of three Surgical Grade 5 titanium alloy (i.e., Ti-6Al-4V, a.k.a. "Ti64")

fracture, bending, and wear have been reported due to stress concentration-induced fatigue failure and stress shieldinginduced aseptic loosening. Long-term follow-up studies have reported that up to 40% of patients, treated with a percutaneous implant, undergo a fixture revision and component exchange [7]. More specifically, stress shielding-induced bone remodeling and resorption, caused by a mismatch between the elastic modulus of the intramedullary implant and the surrounding bone, have been observed in transfemoral amputation patients with percutaneous implanted devices [9], [10]. When comparing *Ti64* alloy, commonly used in skeletal

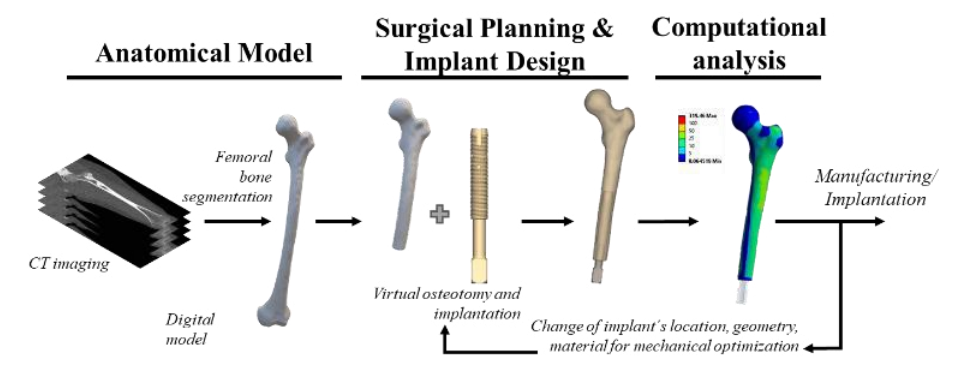


Figure 2. Virtual Surgical Planning (VSP) workflow for the implantation of a transfemoral percutaneous device

components: an intramedullary component, an abutment, and an abutment screw. Much like a dental implant, the OPRATM is most commonly put in place through two surgeries. First, the threaded intramedullary component is inserted and left unloaded for six months, expecting good osseointegration due to the nanoporous surface treatment introduced on the implant (BioHelixTM) [5], [6]. Next, the percutaneous abutment is press-fitted to the distal end of the implant and connected to the prosthetic limb through the abutment-retaining bolt. Better mobility and enhanced sensory feedback are perceived with the use of this type of lower-limb implant, compared to socketsuspended prostheses [7], [8]. Nevertheless, fixation

devices, and the cortical femoral bone, there's an order of magnitude difference in terms of stiffness; the former features an elastic modulus of around 110 GPa, while the latter has a modulus of 16.61±1.83 longitudinally, and 9.55±1.36 transversally in the diaphysis area [11]. Hence, much of the surrounding bone is prevented from receiving sufficient strain, essential for healthy, bone mass-sustaining remodeling.

Reported observations of TFA percutaneous intramedullary prosthetic abutment failure [7], document the need for enhancing and optimizing the structural properties of these devices to 1) withstand the normal physiological, or even accidental, highest load without incurring failure, and 2) not



Figure 1. Osseointegrated Prostheses for the Rehabilitation of Amputees (OPRA TM) Implant System. Assembly shows the three different components.

interfere with the normal stress-strain trajectories through careful design [12].

Previous studies have demonstrated that changing the percutaneous implant's geometry and material can promote or reduce stress shielding. Tomaszewski et al. report that changing the implant's length has a direct effect on load transfer [13]. Similarly, Prochor et al. found that the implant's diameter and length affect bone remodelling [14]. Additionally, in a different study, results showed that the combination of an intramedullary component with a lower elastic modulus and a percutaneous abutment with a higher elastic modulus had beneficial effects on bone maintenance [15]. To the authors' best knowledge, no work has been done on matching either interface's mechanical properties to what is needed to maintain normal stress-strain trajectories or the effect of the implant's location versus its shape.

Novel stiffness-matching approaches for skeletal replacement devices focus on changing the implant's geometry, material, and location [12], to ensure device structural strength and restoration of the normal bone strainstress distribution under *in vivo* loading as well as the overall segment's (e.g., femur, knee, lower leg) function.

Over the last decade, one of the most common research topics for load-bearing skeletal reconstruction devices has been the use of novel biocompatible metallic alloys, such as promising near-equiatomic Nickel-Titanium (NiTi) alloys. The elastic modulus of these alloys is around 40 GPa [16]. Furthermore, Ni-rich NiTi alloys show characteristic reversible solid-state phase transformation, which allows them to undergo large strain levels (up to 8%) without occurring plastic deformation [17].

While a certain level of customization is potentially possible for a percutaneous device such as the OPRATM[6], physicians usually do not have access to the decision-making design process or a vendor willing to fabricate a personalized device. The lack of relevant patient-specific biomechanical 68

information, thus, results in physicians basing their assessment on their experience and published evidence about skeletal reconstruction devices [7].

The study presented here is a Virtual Surgical Planning (VSP) environment, that simulates the mechanical performance of a TFA percutaneous implant. Our VSP environment is based on computer-aided design (CAD) and engineering (CAE) tools, to offer the physician information

about the patient's anatomy and the design of the implant. Moreover, the VSP offers information about the implant's potential mechanical performance under static loading, representing the forces at a time point in the gait cycle, by employing a simplified model. Furthermore, we assess a potential choice by the surgeon between the same devices fabricated from surgical grade titanium (i.e., *Ti64*), and a superelastic material (i.e., *NiTi*). We compare the effect of both materials on the alteration of the stress-strain trajectories in the implanted amputee's adjacent bone.

2. Materials and Methods

2.1. Virtual Surgical Planning

Our VSP environment comprises three stages, as shown in Figure 2. The first step is the creation of a patient's anatomical bone model, either complete or transected femur, from a 3D medical image (i.e. Computerized Tomography [CT]). Second, the bone is digitally transected, and the OPRATM implant is virtually placed. Finally, the device material is chosen, and the implant is computationally tested under relevant static in vivo loading conditions via Finite Element Analysis (FEA). Based on that FEA, it is possible to give feedback, recursively, to the second step in order to optimize the stress distribution in both the bone (increasing it) and the implant (reducing it) by altering the device's shape, material, or implantation location.

2.2. Anatomical model

De-identified CT images of a left leg, containing the whole femur, were obtained from The Ohio State University Radiology Department's Honest Broker System, and exported into Amira 3D 2 022.1 (Thermo Fisher Scientific, Waltham, MA, US) software, where the femoral bone was segmented from the other components of the scan (i.e., muscle, fat, air, etc.). This process was done first using an automatic multithresholding tool to detect and categorize the materials, in every CT slice image, depending on the range and level of tissue density. Next, the segmentation is refined manually. Afterward, the surface of the volume of interest (i.e., bone) is reconstructed and exported as a stereolithography (STL) file.

2.3. Virtual osteotomy and digital device implantation

A digital model of the OPRATM, including the intramedullary and the percutaneous abutment component, was reverse-engineered in SolidWorks 2022 (Dassault Systèmes, Vèlizy-Villacoublay, France) software. These two components were assumed and designed as one component as the study focuses on the interaction between the implant systems and the



Figure 3. Model of the transected femur and implanted with percutaneous implant showing the level of the amputation, and the location of the implant Boundary conditions on FE model. Displacement restraint was applied to the femoral head, while force and moment were applied distally.

bone, rather than the implant itself [18]. The abutment screw was not included in the model.

The implant and bone models were imported into Freeform 2022.1.32 (3D Systems, Rock Hill, SC, US) to perform the virtual osteotomy and digital implantation of the device (shown in Figure 3).

The trans-femoral cut was done 250 mm above the knee (i.e., mid-diaphysis). The intramedullary portion of the implant was positioned vertically, leaving 20 mm between the distal thread and the distal transected end of the femur [6].

2.4. Finite Element Analysis

The assembly, including bone and implant, was imported into ANSYS Workbench 2022 R2 (Canonsburg, PA, US) software for FEA setup, component meshing, and model solving. Also, the femur in healthy condition, was tested under the same loading conditions to assess the changes in the stressstrain trajectories caused by the introduction of the metallic implant OPRATM implant.

The mechanical properties of the materials assigned to the components are shown in Table 1. For model simplification, the materials' properties were considered homogeneous and isotropic. Bone and Ti64 were modelled as linear elastic materials. Moreover, the femur was assumed to be composed only of cortical bone. This assumption is commonly taken in regard to the femur to reduce the computational expense. On the other hand, NiTi was modeled using the ANSYS superelastic model, to accurately simulate the stress-induced phase transformation. Besides the elastic modulus, the material model has as input the martensite start and martensite finish stress values (σ_{SAS} , σ_{FAS}), and the recovery strain (ε). *NiTi* mechanical properties were obtained from experimental data.

Table 1. Material properties are assigned to the components in the FEA.

Material	Elastic Modulus, E (GPa)	Poisson ratio, v	σsas (MPa)	σ _{FAS} (MPa)	ε (mm/mm)
Bone [19]	17.00	0.30	-	-	-
Ti64 [20]	115.00	0.30	-	-	-
NiTi	16.58	0.30	72.20	116.66	0.018

The contact between the threaded area of the implant and the bone was set as bonded (tied) to model the screw in the area joining the components and assuming ideal full implant-bone integration, thus preventing any local normal or tangential relative motion [21]. The contact between the bone and the implanted section of the abutment was set as frictional with a factor of 0.2 [10].

The boundary conditions applied to the model, shown in Figure 3, simulate the static force shortly before toe-off, at approximately 55% of the gait cycle [3], [8]. The loading is representative of a body of 100 kg, which included 90% of the study population weight [7]. Both conditions were selected to evaluate the implant under extreme conditions. The loading magnitude and direction, presented in Table 2, were experimentally measured on an instrumented knee prosthesis and an instrumented percutaneous implant, for an intact and a percutaneous-implanted femur, respectively, and scaled to a 100 kg body mass [8]. For the healthy model, the loading conditions were applied to the femoral condyles, assuming symmetrical force transferring. In the implanted case, the loading conditions were applied to the distal end of the implant. The displacement and rotation of the element nodes on the femur-acetabulum joint area on the femoral head were restrained in all 6 degrees of freedom (DOF) [22].

Table 2. Loading conditions for intact and implanted bone.

			1			
	$F_x(N)$	$F_y(N)$	$F_z(N)$	M _x (Nm)	My (Nm)	Mz (Nm)
Intact femur	-99	73	1913	-40	60	20
OPRA implanted	66	196	295	6.7	61.0	0.0

Tetrahedral elements were employed to build the FE volumetric mesh. After an element sensitivity test was performed to reduce the maximum stress difference to below 2% of the previous coarser mesh, the femur consists of 232,426 elements with a minimum size of 1.00 mm, while the implant contains 936,440 elements with a minimum size of 0.50 mm.

3. Results

Figure 4 a) and d) show a front and a cross-section view, respectively, of the stress distribution of the intact bone under static loading conditions. We observe similar results to those presented by Tomaszewski et al. [8]. The largest stress values are found in the femoral neck and along the diaphysis. In the cross-section view (Figure 4 d), stress concentrates in the outer areas, while a neutral stress path can be found along the midsection of the shaft.

The stress distribution, after implanting the *Ti64* and *NiTi* percutaneous devices on the transected femur, can be observed in Figure 4 b), c) and Figure 4 e), f), respectively (i.e., frontal and cross-sectional views, respectively). Although there is a physiologically relevant stress concentration at the femoral neck, and the cross-section shows similar stress pathways of the implanted femur, it is noticeable that the stress pattern along

the bone shaft is altered and reduced, compared to the healthy condition. Our model suggests that most of the area around the

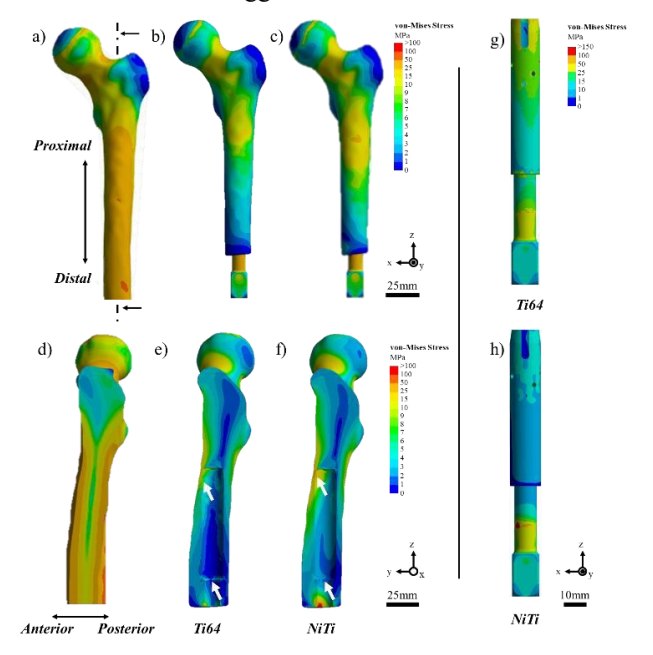


Figure 4. Von Mises stress distribution in a), and d) intact bone; b), and e) *Ti64*-implanted bone; and c), and f) *NiTi*-implanted bone. The dotted line in a) shows the plane for the cross-section view in d-f. White arrows on figures e) and f) show the location of the stress measurement.

implant gets unloaded, with Von Mises stress values reducing as it gets from the proximal to the distal end of the bone. Furthermore, new stress concentration areas appear with the device implantation, as seen at the distal bone edge, due to the interaction between both components.

A reduction in the stress transferred to the bone is more noticeable with the implantation of a *Ti64* device (Figure 4 b) and e)), rather than a *NiTi* implant (Figure 4 c) and f)). The highest stress value in the upper periprosthetic bone around the *Ti64* implant is 16 MPa, while with the use of a *NiTi* device, the stress value at the same point is 26 MPa (63% higher), as pointed out by the upper arrows. Other works have reported between 15 MPa to 23 MPa in the proximal perisprosthetic bone [14], [23].

On the distal end (pointed out by the lower arrows), the load on the bone nearby increases from 0.44 MPa to 1.97 MPa, 2.20 times higher. Thus, we observe that the stress in the host bone tends to be restored with the use of a less stiff material. Previous works have reported similar behavior in the distal and proximal bone, with stress values between 3 to 40 MPa [3], [10].

When analyzing the stress distribution in the implant, shown in Figure 4, for *Ti64* g) and *NiTi* h), the FEA suggests the less stiff *NiTi* promotes an overall reduction in localized stress concentration, compared to *Ti64*. Not surprisingly, and as in previous studies [20], the section of the abutment not in contact with the bone shows increased stress between both materials and a localized stress concentration due to the adjacent interaction between the bone and the device (Figure 4 e) and f)). The resulting Von Mises stress in NiTi shows a maximum value of 75 MPa, in the percutaneous abutment. Hence, the localized stress is in the elastic phase transformation range and

below the plastic yield strength, suggesting the device will not fail under the loading conditions.

7

4. Discussion

This work is motivated by the desire to overcome the limited information that physicians currently have in planning, deploying, and tracking outcomes, concerning: 1) the patient's three-dimensional anatomy, 2) the best location of the implant in terms of mechanical performance, and 3) evidence for decisions on a mid-diaphysis, transected, femoral percutaneous implant's geometry and material.

Allowing the bone adjacent to an OPRATM implant to experience dynamic strain is a crucial factor for osseointegration, and bony tissue growth and maintenance [24]. Even though initial osseointegration and neglectable implant migration have been reported at early stages [4], skeletal devices for reconstruction or replacement, are commonly stiffer than bone, promoting stress-shielding, periprosthetic bone resorption, and implant failure. Stress shielding is observed in several lower limb implants such as femoral condyle endoprosthesis (FCE) [25], total hip arthroplasties (THA) [26], total knee replacement (TKR), and percutaneous implants [27].

In this work, the use of a virtual surgical planning (VSP) environment was presented for planning and deploying a transfemoral implant of a commercial percutaneous device. In addition to planning the surgery (i.e. osteotomy location), our VSP environment allows for advanced procedure and skeletal fixation device design (i.e., device material, external and internal geometry, and anatomical location), and mechanical modelling of the skeletal implant's anticipated performance. Hence, this approach not only personalizes the implant shape but its mechanical performance as well. The application of this VSP has been reported in our previous work for craniomaxillofacial (CMF) devices [28].

As with most osseointegrated implants, there needs to be time for bone growth around the device. However, in patients treated with percutaneous implants, one can expect the presence of osteoporotic bone, due to the extended time without loading the skeletal tissue [29]. Furthermore, aged patients, in comparison to younger ones, tend to present wider femoral canals [30]. Besides offering weaker anchoring areas, these factors will also promote bone resorption, by enlarging the stiffness mismatch. Hence, being able to design an intramedullary component, with a proper diameter that reaches a strong dense bone cortex, will benefit the prosthesis anchoring.

In addition to geometry, the implant's material plays a major role in the overall stiffness. The computational results presenting the load transfer between the bone and the implant following osseointegration, under static loading, compare two different biocompatible materials: *Ti64* and *NiTi*. The comparison highlights the importance of this design variable. Less stiff materials will allow larger displacement under

loading, hence more stress transferred to the bone-stimulating bone-sustaining remodelling. *NiTi* alloys have been commonly used in small medical devices, such as wires, nails, staples, and stents [31]. The development of larger and bigger medical devices is limited by the challenging processing of these alloys via conventional means. However, advanced manufacturing techniques, such as Laser-Based Power Bed Fusion, result in high density, near-net shape, and outstanding properties [32]. Furthermore, additive manufacturing techniques allow stiffness-matched personalized devices [12].

Finally, assessing the optimal implant's location dramatically affects the performance. Besides evaluating the stress transferring between bone and implant, detecting stress concentration areas and stress pattern changes can also give information about how the device location plays a role in potential failure [12], [33]. In this study, we observe stress concentration (on the cross-section view) in the bone, which we believe is due to the thin residual bone provoked by the countersunk distance in the bone. Previous work has also shown radiographic images with thin bone surrounding the implant [4], [13], [34]. Nevertheless, the resulting maximum stress in bone, observed in the NiTi-implanted case (26 MPa), is lower than the bone strength (S=160.5 MPa) [20]; thus, it does not invalidate its stability by staying below the plastic deformation threshold, assuming isotropic properties. However, it is known that mechanical properties in the radial and transverse directions are lower than in the longitudinal axis [35]. On the other hand, implantation length will affect the overall deformation, as the lever arm will be changed, changing the flexion [10]. To the authors' best knowledge, the mechanical assessment of the location of percutaneous implants has not been fully reported.

Further work, considering different geometries, materials, and locations for the OPRATM of the implant, may allow us to overcome the current limitations identified in our computational model. The accuracy of the model will be improved by taking into account factors such as bone remodelling [23], and muscle interaction [36] that were not considered in this study. Moreover, it has been reported that the implant/tissue interface plays a crucial factor in cortical stress and implant stability [37]. To address the latter, the FEA would consider non-linear friction contacts, and a larger number of elements and nodes, increasing the model complexity and computational time. Additional limiting factors are the generalization of the bone's mechanical properties and characteristics, since it is known that they depend on the patient's age, type of bone tissue, mineral content, level of porosity, and loading direction [38]. Furthermore, reported mechanical values in literature might differ from the in vivo performance, and among studies due to differences in testing conditions [39]. Additionally, plastic deformation, inhomogeneities, and anisotropy of the OPRATM parts under loading conditions will be further investigated.

5. Conclusions

We anticipate that offering the physician and engineering design team information about the personalized mechanical performance of a medical device by assessing its geometry, material, and location, will have a positive impact on the patient's post-operative well-being. Herein, we study the application of these principles for patients who are treated with a percutaneous transfermoral implant. Furthermore, it was assessed the load transfer from the implant to the healed bone by switching the standard-of-care *Ti64* to *NiTi*. Conclusions from the study reported here include:

- Less stiff materials can help restore the normal physiological bone distribution in the bone. However, they might reduce the load-bearing potential of the device.
- The geometry and location of the implant play an important role in the stiffness matching approach since it will affect the load transferring and the promotion of stress concentration.

Further work will be done to enhance the computational model so that the effect of different design parameters of novel and commercially available percutaneous implants can be addressed.

Acknowledgments

Authors acknowledge support from an Ohio State University (OSU) President's Research Excellence (PRE) Catalyst Grant, OSU James Comprehensive Cancer Center Biomedical Device Initiative grant, and a National Science Foundation (NSF) Hybrid Autonomous Manufacturing, Moving from Evolution to Revolution (HAMMER)

Engineering Research Center (ERC) grant, NSF EEC2133630. The authors thank Athena Zhang, MD; Kenzington Kottenbrock, and Saylor Priest, for acquiring de-identified medical scans from OSU Honest Broker radiological service.

References

- [1] Perkins, Z. B., De'Ath, H. D., Sharp G., Tai N. R. M., 2011. Factors affecting outcome after traumatic limb amputation, British Journal of Surgery, vol. 99, pp. 75–86.
- [2] Childress, D., 1997. The interfaces between humans and limb replacement components, in International Workshop on Osseointegration in Skeletal Reconstruction and Joint Replacement, Quintessence Pub Co.
- [3] Xu, W., Xu, D. H., Crocombe, A. D., 2006. Three-Dimensional Finite Element Stress and Strain Analysis of a Transfemoral Osseointegration Implant, Proc Inst Mech Eng H, vol. 220, pp. 661–670
- [4] Nebergall, A., Bragdon C., Antonellis, A., et al., 2012. Stable fixation of an osseointegrated implant system for above-the-knee amputees, Acta Orthop, vol. 83, pp. 121–128
- [5] Brånemark, R., Emanuelsson, L., Palmquist, A., Thomsen, P., 2011. Bone response to laser-induced micro- and nano-size titanium surface features, Nanomedicine, vol. 7, pp. 220–227
- [6] Thesleff, A., Brånemark, R., Håkansson, B., Ortiz-Catalan, M., 2018. Biomechanical Characterisation of Bone-anchored Implant Systems for Amputation Limb Prostheses: A Systematic Review, Ann Biomed Eng, vol. 46, pp. 377–391
- [7] Hagberg, K., Ghassemi Jahani, S.-A., Kulbacka-Ortiz, K., Thomsen, et al., 2020. A 15-year follow-up of transferoral amputees with bone-anchored transcutaneous prostheses, Bone Joint J, vol. 102-B, pp. 55–63

- [8] Tomaszewski, P. K., Verdonschot, N., Bulstra, S. K., Verkerke, G. J. 2010. A Comparative Finite-Element Analysis of Bone Failure and Load Transfer of
 - Osseointegrated Prostheses Fixations, Ann Biomed Eng, vol. 38, pp. 2418–2427
- [9] Tsikandylakis, G., Berlin, Ö., Brånemark, R., 2014. Implant Survival, Adverse Events, and Bone Remodeling of Osseointegrated Percutaneous Implants for Transhumeral Amputees, Clin Orthop Relat Res, vol. 472, pp. 2947–2956
- [10] Stenlund, P., Trobos, M., Lausmaa, J., et al., 2017. Effect of load on the bone around bone-anchored amputation prostheses, Journal of Orthopaedic Research, vol. 35, pp. 1113–1122
- [11] Neil Dong, X., Edward Guo, X., 2004. The dependence of transversely isotropic elasticity of human femoral cortical bone on porosity, J Biomech, vol. 37, pp. 1281–1287
- [12] Chmielewska A., Dean, D., 2023. The Role of Stiffness-Matching in the Design of Metallic Skeletal Reconstruction Devices- a Review, Acta Materalia, Inc, vol. 173, pp. 51-65
- [13] Tomaszewski, P. K., Verdonschot, N., Bulstra, et al., 2012. Simulated bone remodeling around two types of osseointegrated implants for direct fixation of upper-leg prostheses, J Mech Behav Biomed Mater, vol. 15, pp. 167– 175
- [14] Prochor, P., Sajewicz, E. 2019. The Influence of Geometry of Implants for Direct Skeletal Attachment of Limb Prosthesis on Rehabilitation Program and Stress-Shielding Intensity, vol. 2019, pp. 1–17
- [15] Prochor, P. Frossard, L., Sajewicz, E. 2020. Effect of the material's stiffness on stress-shielding in osseointegrated implants for bone-anchored prostheses: a numerical analysis and initial benchmark data, Acta Bioeng Biomech, vol.2, pp. 69-81
- [16] Petrini, L., Migliavacca, F., 2011. Biomedical Applications of Shape Memory Alloys, Journal of Metallurgy, vol. 2011, pp. 1–15
- [17] Taheri Andani, M., Haberland, C., Walker, J. M., et al., 2016. Achieving biocompatible stiffness in NiTi through additive manufacturing, J Intell Mater Syst Struct, vol. 27, pp. 2661–2671
- [18] Lee, W. C. C., Doocey, J. M., Brånemark, R., et al., 2008. FE stress analysis of the interface between the bone and an osseointegrated implant for amputees – Implications to refine the rehabilitation program, Clinical Biomechanics, vol. 23, pp. 1243–1250
- [19] Sun, Y., Xu, S., Ly, S., et al., 2022. Extramedullary Osseointegration—A Novel Design of Percutaneous Osseointegration Prosthesis for Amputees, Front Bioeng Biotechnol, vol. 10
- [20] Mirulla, A. I., Di Paolo, S., Di Simone., F., et al., 2020. Biomechanical Analysis of Two Types of Osseointegrated Transfemoral Prosthesis, Applied Sciences, vol. 10, p. 8263
- [21] Thesleff, A., Ortiz-Catalan, M., Brånemark, R., 2022. The effect of cortical thickness and thread profile dimensions on stress and strain in boneanchored implants for amputation prostheses, J Mech Behav Biomed Mater, vol. 129, p. 105148
- [22] Goh, B. T., Lee, S., Tideman, H., Stoelinga, P. J. W. 2008. Mandibular reconstruction in adults: a review, Int J Oral Maxillofac Surg, vol. 37, pp. 597–605
- [23] Ghaziani, A. O., Soheilifard, R., Kowsar, S., 2021. The effect of functionally graded materials on bone remodeling around osseointegrated trans-femoral prostheses, J Mech Behav Biomed Mater, vol. 118, p. 104426
- [24] Ehrlich, P. J., Lanyon, L. E. 2002. Mechanical Strain and Bone Cell Function: A Review, Osteoporosis International, vol. 13, pp. 688–700
- [25] Wik, T. S., Foss, O. A., Havik, S., et al., 2010. Periprosthetic fracture caused by stress shielding after implantation of a femoral condyle endoprosthesis in a transfemoral amputee—a case report, Acta Orthop, vol. 81, pp. 765–767
- [26] A. H. Glassman, J. D. Bobyn, and M. Tanzer, "New Femoral Designs,"
 - Orthop Relat Res, vol. 453, pp. 64–74, Dec. 2006, doi: 10.1097/01.blo.0000246541.41951.20.
- [27] Li, M. G., Nilsson, K. G., 2000. Changes in bone mineral density at the proximal tibia after total knee arthroplasty: A 2-year follow-up of 28 knees using dual energy x-ray absorptiometry, Journal of Orthopaedic Research, vol. 18, pp. 40–47
- [28] Vazquez-Armendariz, J., Olivas-Alanis, L. H., Mahan, T., et al., 2023. Workflow for Robotic Point-of-Care Manufacturing of Personalized Maxillofacial Graft Fixation Hardware, Integr Mater Manuf Innov, vol. 12, pp. 92–104
- [29] Sherk, V. D., Bemben, M. G., Bemben, D. A., 2008. BMD and Bone Geometry in Transtibial and Transfemoral Amputees, Journal of Bone and Mineral Research, vol. 23, pp. 1449–1457

- [30] Glassman, A. H., Bobyn, J. D., Tanzer, M., 2006. New Femoral Designs, Clin Orthop Relat Res, vol. 453, pp. 64–74
- [31] Yang, C., Abanteriba, S., Becker, A., 2020. A review of shape memory alloy based filtration devices, AIP Adv, vol. 10
- [32] Jahadakbar, A., Nematollahi, M., Safaei, K., et al., 2020. Design, modeling, additive manufacturing, and polishing of stiffness-modulated porous nitinol bone fixation plates followed by thermomechanical and composition analysis, Metals (Basel), vol. 10
- [33] Olivas-Alanis, L. H., 2023. Implementation of advanced design and additive manufacturing techniques for the development of medically relevant devices, Tecnologico de Monterrey, Monterrey, 2023.
- [34] Palmquist, A., Windahl, S. H., Norlindh, B., et al., 2014. Retrieved boneanchored percutaneous amputation prosthesis showing maintained osseointegration after 11 years—a case report, Acta Orthop, vol. 85, pp. 442– 445
- [35] Morgan, E. F., Unnikrisnan, G. U., Hussein, A. I., 2018. Bone Mechanical Properties in Healthy and Diseased Stated, Annu Rev Biomed Eng, vol. 20, pp. 119-143
- [36] Speirs, A. D., Heller, M. O., Duda, G. N., Taylor, W. R. Physiologically based boundary conditions in finite element modelling, J Biomech, vol. 40, pp. 2318–2323
- [37] Castrillo, G., Carnicero, A., Perera, R., 2023. Submodelling approach to screw-to-bone interaction in additively manufactured subperiosteal implant structures, Int J Numer Method Biomed Eng, vol. 39
- [38] Currey, J. D., 2004. Tensile yield in compact bone is determined by strain, post-yield behaviour by mineral content, J Biomech, vol. 37, pp. 549–556
- [39] Sedlin, E. D., Hirsch, C. 1996. Factors Affecting the Determination of the Physical Properties of Femoral Cortical Bone, Acta Orthop Scand, vol. 37, pp. 29–48